Assessing Resolution in Super-Resolution Imaging

Justin Demmerle [a], Eva Wegel [a,b], Lothar Schermelleh [a], Ian M. Dobbie [a,*]

[a.] Micron Advanced Bioimaging Unit, Department of Biochemistry, University of Oxford, South Parks Road, Oxford OX1 3PT, United Kingdom
[b.] Current address: Bioimaging Facility, John Innes Centre, Norwich Research Park, Colney, Norwich NR4 7UH, United Kingdom
* Email: ian.dobbie@bioch.ox.ac.uk; Tel: +44 (0)1865-613323

Abstract

Resolution is a central concept in all imaging fields, and particularly in optical microscopy, but it can be easily misinterpreted. The mathematical definition of optical resolution was codified by Abbe, and practically defined by the Rayleigh Criterion in the late 19th century. The limit of conventional resolution was also achieved in this period, and it was thought that fundamental constraints of physics prevented further increases in resolution. With the recent development of a range of super-resolution techniques, it is necessary to revisit the concept of optical resolution. Fundamental differences in super-resolution modalities mean that resolution is not a directly transferrable metric between techniques. This article considers the issues in resolution raised by these new technologies, and presents approaches for comparing resolution between different super-resolution methods.

1. Introduction

Microscopic images at the theoretical limit of optical resolution have been available for well over 100 years. Recently, the diffraction limit has been overcome by a number of new optical imaging techniques, collectively known as super-resolution microscopy[1,2]. Two critical questions pose themselves to scientists interested in applying these new technologies. Firstly, what is the actual resolution of the resulting image? Secondly, is the increased effort and expense of super-resolution, as compared to conventional microscopy, worth the increase in resolution? The recent introduction of a range of commercial super-resolution instruments means that resolution has once again become a battleground between different microscope technologies and rival companies.

In this paper we classify super-resolution microscopy into three broad classes and assess the achievable resolution in each. As different super-resolution techniques produce images that are amenable to different methods of resolution measurement, we consider these different measurement methods, to which super-resolution microscopy methods they can reasonably be applied, and address some possible artifacts in their application. We also provide metrics for a realistic expectation of achievable resolution using relatively standard techniques and commercially available instruments (Table 1). In all cases these resolutions have been surpassed, but measurements from standard biological samples, with commercially available equipment, are a useful comparison for assessing the relative merits of different super-resolution techniques.

It should be noted that resolution is a multifaceted concept, and that measuring it is not as trivial as it may appear. To meaningfully compare different techniques it is essential to specify the exact definition of the resolution one is measuring. Further, resolution is only one of many contributors to the utility of a given microscopy technique. There are also a number of external factors such as sample labeling and signal to noise ratio that can also affect image quality. While these do not change the system's resolution, such factors significantly affect the overall image quality, even if the resolution is still extremely high.

2. Material and Methods

2.1 Sample Preparation

Drosophila macrophages were prepared from third instar larvae as previously described [3]. Cells were prepared for imaging with an immunofluorescence protocol modified for macrophage microtubules (Wegel et al., manuscript in preparation), with monoclonal mouse anti α-tubulin (Sigma-Aldrich T6199, clone DM1A) primary antibody, and polyclonal donkey anti mouse AlexaFluor 488 (Life Technologies A11015) secondary antibody. Samples were embedded in Prolong Gold (Life Technologies P36930) and cured for 16-20 hours before sealing.

2.2 Microscopy

2.2.1. Stuctured Illumination Microscopy (SIM), Widefield, and Widefield-deconvolution data

SIM data was generated on a DeltaVision OMX V3 Blaze system (GE Healthcare) equipped with a 63x 1.42 N.A. PlanApo oil immersion objective (Olympus), a 488 nm diode laser, and Edge 5.5 sCMOS cameras (PCO). Image stacks of ~5 μm were acquired with a z-distance of 125 nm and with 15 raw images per plane (five phases, three angles). Raw datasets were computationally reconstructed with a channel-specific measured optical transfer function (OTF) and a Wiener filter set to 0.002 using the softWoRx 6.1 software package (GE Healthcare). Widefield data was generated by averaging all phases and angles for each slice of the raw SIM dataset, using the SIMcheck plugin suite for ImageJ (Ball et al., manuscript submitted). Widefield-deconvolution data was generated by taking the widefield image and deconvolving with softWoRx 6.1 software.

2.2.2. gated STimulated Emission Depletion (gSTED) data

gSTED data was generated on a SP8 gated STED system (Leica), equipped with a HCX PlanApo 100x 1.40 N.A. oil immersion objective (Leica), 488 nm argon laser, and standard PMT detectors. Probes were excited with a pulsed 488 nm laser and depleted with a 592 nm STED laser. Images were acquired with Leica LAS AF software's TCS SP8 module.

2.2.3. direct Stochastic Optical Reconstruction Microscopy (dSTORM) data

dSTORM data was generated with a modified DeltaVision OMX V2 system (GE Healthcare) equipped with a 100X PlanApo 1.40 N.A. oil immersion objective (Olympus), a 488 nm diode laser, Evolve 512 Delta EMCCD cameras (Photometrics), and a customized lightpath with approx. 30 kW/cm^2 laser intensity. 4000 images were acquired in widefield illumination with an integration time of 50

ms. Localizations were produced with fastSPDM, a maximum-likelihood-based algorithm with a sliding window for background subtraction [4], and adapted to the hardware configuration of the microscope. Super-resolution images were generated from the position data based on nearest-neighbor distances in order to account for label density effects limiting the resolution [5].

2.3. Analysis

Fourier spectra were generated using the SIMcheck FFT function in the Fiji implementation of ImageJ [6,7] as this applies a Gaussian windowing of 6% of the image width prior to padding with zeros to reduce edge artifacts in the resulting FFT images. The power spectrum, the amplitude squared of the complex FFT, is log scaled in order to enable visualization of the high central peak and the low intensities near the noise floor. These images were then radially averaged around the center to generate FFT line profiles using Paul Baggethun's Radial_Profile plugin: http://rsb.info.nih.gov/ij/plugins/radial-profile.html. These radial profiles show how information in the image is distributed across different resolutions, clearly showing how structures at different sizes are represented in the image and allowing assessment of the image resolution. The resultant FFT images were scaled so that the equivalent spatial resolution was at the same distance from the center point.

Resolution measurement from microtubules were taken in ImageJ. Line profiles of single microtubules integrated over a width of 165 nm in all image types were taken. The Full Width Half Maximum (FWHM) of these profiles was then extracted. To improve sensitivity the line profiles were fitted with a Gaussian and the Full Width Half Maximum (FWHM) was calculated as for the resultant Gaussian as $2\sqrt{(2 \ln 2)}\sigma$, where σ is the Gaussian width parameter.

3. Measuring resolution

There is a dichotomy between the theory and practice of resolution in optical microscopy. The theoretical approach is almost universally based upon the Rayleigh Criterion [8], whereby the resolution is defined as the distance at which the first trough in the Airy disk of one point object falls exactly on the peak of another. This is calculable from Airy's original theory [9] and works out as the classic resolution limit of $1.22\lambda / 2NA$, where λ is the wavelength and NA is the system's numerical aperture (for epi-fluorescence, in transmission the denominator becomes (NA_{cond}+NA_{obj}), where NA_{cond} is the condenser NA and NA_{obj} the objective NA). This is equivalent to a contrast limit of about 25*%, i.e.* there is an ~ 25% dip in intensity between the two peaks and the trough between them. In practice, the resolution is usually measured as the Full Width Half Maximum (FWHM) of a point object, such as a sub-resolution fluorescent bead. To improve the sensitivity of these measurements, the single peak is then usually fitted with a Gaussian distribution (see section 2.3).

Another resolution definition, which may be thought to be more representative of achievable resolution in a system, is the Sparrow Criterion [10]. Briefly, this is similar to the Rayleigh Criterion, but says that objects are distinguishable until there is no dip between the peaks. This has two major drawbacks over the Rayleigh criterion: 1)

it is very signal-to-noise dependent, and 2) it has no easy comparison to a readily measured value in real images, such as the FWHM for the Rayleigh Criterion.

The theoretical and practical approaches are fundamentally different; however in practice the results are similar, as the FWHM is similar to the distance between the peak and the first trough of a real Airy disk. Critically, this depends upon the shape of the Point Spread Function (PSF). A Gaussian is generally a good approximation of the point spread function of a microscope objective, so equating these different measurements is reasonable. It should be noted that this is an approximate equality, and so extra care should be taken in extreme circumstances such as super-resolution imaging.

The underlying reason for the difference between the theoretical and practical approaches is that the theoretical approach aims to precisely calculate the achievable resolution of a real system, whereas the practical approach aims to be simple and robust. If one, *a priori,* knows that there are two point sources, then measuring their separation, and hence calculating the system's resolution is purely limited by Signal to Noise ratio (S:N). The Rayleigh Criterion is a realistic rule of thumb, giving an approximate measure of the smallest object resolvable in a well-calibrated optical microscope. However, with additional information, such as the fact that there is a single point object in a given region, significantly more accurate results can be obtained. This is the fundamental basis behind Single Molecule Localization Microscopy (SMLM) based techniques, and one reason why "system resolution", "localization precision", and "image resolution" are not identical.

Traditionally, approximating the resolution of a conventional microscope with the FWHM of a Gaussian fit to a PSF (the image of a single sub-resolution point source) is a good approximation of realistically achievable system performance. Super-resolution microscopy makes this issue significantly more complicated, and adds several additional factors to an area that is already difficult to navigate. For this reason we start with an overview of resolution in conventional systems.

3.1 Widefield Resolution

To evenly compare the various super-resolution techniques with widefield microscopy, and with each other, we will only consider the various techniques when used for fluorescence imaging, in as optimal of conditions as is reasonably possible. The samples will be either small (~100 nm) beads, in some high refractive index mounting media, or biological samples labeled with a relatively bright and photo-stable dye (such as Alexa488) and imaged near the coverslip in high refractive index mounting media.

The classical theoretical resolution in widefield microscopy is given by the Rayleigh Criterion and for excitation at 488 nm, emission around 515 nm, and with a 1.40 NA oil immersion objective, the theoretical resolution is (1.22*500)/(2*1.4) ≈ 220 nm. Similar values can be gained from biological samples such as antibody-stained microtubules (Table 1). Further examples will use these samples for all techniques, starting with widefield microscopy, including its combination with deconvolution (Fig. 1A and B).

A useful method of extracting information about the system's resolution, and more importantly, relative information content at different length scales, is to look at Fourier transforms, which we term Fourier Spectrum Analysis. The intensity component of the Fourier transform clearly shows how information in the sample is transferred into the image. A widefield image has overall circular symmetry in its Fourier transform, although noise or specific image features mean it is not truly symmetric (Fig. 2A). The rate at which the information content decreases with scale can be best assessed by integrating around the circle at equal distance from the center, a radial average, of the Fourier transform to give a simple line plot of information content against inverse length (Fig. 3). It should be noted that the Fourier transform must be created with the zero frequency at the center for this to work. Care must be taken in interpreting such graphs as the absolute scale is difficult to normalize, and the x-axis, inverse length, is non-linear. The circular region where the information content vanishes into the background noise is, essentially, the resolution limit achievable by the system, and drops off at the frequency equivalent of 0.2 μm in widefield images, although deconvolution significantly improves information transfer at these high frequencies (Fig. 2A and B). This approach allows assessment of resolution on more complicated, and possibly more relevant, samples than sub-resolution beads, as well as giving a measure for the image as a whole as opposed to measuring resolution at isolated regions.

It should be noted that it is also informative to look at the Z-resolution of a 3D image stack, where applicable. It has previously been noted that systems often exceed the theoretical Z resolution, and this can be due to approximations in the theoretical treatment [11]. As well as measurements such as FWHM of a fitted Gaussian, the Z resolution can be assessed by using Fourier transforms of a 3D image stack. This can show both the "missing cone", intrinsic to widefield microscopy [12], and the limited Z resolution compared to that in XY. An additional technique, closer to the theoretical Rayleigh Criterion, is to look at crossed sub-resolution structures, such as microtubules. This will give profiles in X and Y at the resolution limit of the system. By interpolating from several position measurement of each microtubule, before and after the intersection, it is possible to obtain an accurate measure of their separation at any point. Progressive line plots at different distances from their crossover point will demonstrate the separation at which the two filaments are resolvable, thus giving a measure of resolution.

3.2. Super-resolution microscopy

We classify super-resolution techniques into three broad classifications: those based upon Structured Illumination Microscopy (SIM) [12-14] those based upon point spread function engineering such as STED [15,16] and RESOLFT [17] (hereafter referred to as STED); and those based upon localization of individual fluorophores, known by a range of acronyms (PALM, FPALM, GSD, STORM, dSTORM, etc.) [18-20] but now commonly referred to as Single Molecule Localization Microscopy (SMLM). These three classes will be considered individually in order to cover what resolution might mean in each case, and the various methods by which it can be measured.

3.2.1 Structured Illumination Microscopy

In SIM the sample is illuminated by a structured pattern, with dark and bright regions at, or near, the resolution limit. The pattern is then shifted to provide complete illumination of the in-focus plane. Typically this is done by illuminating with stripes and phase-shifting the stripes over a complete cycle [12,21]. Many other schemes are possible, including random patterns [22] or unknown patterns [23]. The data is then processed to extract super-resolution information in the direction of the stripes. The stripes are then rotated to provide information from a range of angles. Typically 3 or 5 different angles are used to provide approximately isotropic resolution enhancement. Additionally, the illumination pattern may have stripes (or other patterns) in the Z direction (3D-SIM) allowing super-resolution information to be extracted in the axial dimension [12]. A related, but not identical, approach is Multi-focal Structured Illumination Microscopy (MSIM), where an array of pinholes is used in confocal mode [24,25]. Images of the pinholes are shrunk by a factor of two either digitally or optically and then combined to build up an image. This technique has considerably simpler image processing than conventional SIM with a $\sqrt{2}$ resolution improvement. The same approaches to measuring resolution in SIM as discussed below apply equally to MSIM and its variants.

3.2.2. Resolution in Structure Illumination Microscopy (SIM)

Measuring resolution in SIM follows a similar approach to that in widefield fluorescence imaging. Theoretical approaches state that in ideal conditions, resolution will be exactly twice that in widefield (≈110 nm in the case calculated in section 3.1). This can be clearly seen in the increased detail visible in microtubule networks (Fig. 1C) and the measure of FWHM as shown in Table 1. The relatively large amount of processing to produce a final super-resolution SIM reconstructed image means that it is not clear from the raw data what the final resolution will be, and it can only be calculated after the final image is generated using the relevant calibration parameters or theoretical data, depending on the system. Additionally, it should be noted that the resolution of SIM data is not truly isotropic, depending on the number of angles used in the reconstruction, with the fewer angles used the higher the anisotropy.

It is useful to examine the Fourier transforms of SIM reconstructions when assessing the resolution (Fig. 2C). These have a very characteristic multi-lobed pattern, depending on the number of angles used in the original imaging, with 3 angles giving 6 lobes and 5 angles giving 10 lobes. The increase in resolution compared to widefield methods is apparent in the information filling the Fourier spectrum in the frequencies between 0.2 μm and 0.1 μm (Fig. 2C).

Care must be taken with using this pattern to assess true structural resolution, as the reconstruction algorithm can easily add background speckle at the resolution limit that is not indicative of true structure. Using the SIMcheck ImageJ plugin (Ball et al., manuscript submitted), we have found that the rate at which the Fourier intensity falls with scale is a critical factor in determining whether the resolution achieved is from actual image features, or is instead noise from reconstruction artifacts. A relatively smooth transition from low frequencies to high frequencies at the resolution limit is indicative of a good reconstruction. An even level of spectra power (*e.g.* a roughly constant region in the FFT between the center and the resolution limit) followed by a sharp fall at the resolution limit usually implies that the information content is actually

noise and not real structure. Using Fourier transforms to assess the Z resolution can be particularly informative, as it clearly shows the filling in of the “missing cone”, leading to the optical sectioning achieved in 3D SIM imaging. With transverse Fourier transforms, the Z resolution is often substantially lower than that in XY, and the Fourier transform can introduce significant edge artifacts, which can be alleviated by using a window function to match the top and bottom edges of the image before transforming. Further, resolution in SIM imaging is often photobleach-limited, as 3D-SIM typically requires at least 15 frames per Z section and multiple, closely space Z sections. Taking repeat images of samples is then extremely difficult, and photobleaching causes a decrease in the S:N that can contribute heavily to artifacts.

3.3.1. Stimulated Emission Depletion (STED)

STED relies upon the ability to switch off the fluorescence in a way that can be saturated in a non-linear manner, with the non-linearity enabling resolution beyond the diffraction limit [16]. Broadly, STED excites a single diffraction limited spot and then stimulates the periphery of the spot to emit at a time or wavelength that is not detected. As long as the stimulated emission beam has a true zero in the exact center of the spot, then extremely high resolutions can be achieved. STED has been performed with both pulsed and continuous depletion beams, and current commercial systems rely upon continuous wave depletion beams, making the equipment significantly cheaper and easier to use. RESOLFT works in a similar manner, activating fluorescence in a diffraction-limited spot and then deactivating fluorescence in a ring around the central peak [17]. Again, if the center of the depletion beam is a true zero then the deactivation can be saturated and extremely high resolutions are possible. A significant issue with STED and related techniques is that generating an image requires exciting and de-exciting a given region a large number of times, so photo-bleaching and photo-damage are almost always the major limiting factor.

3.3.2. Resolution in STED microscopy.

Fundamentally, the resolution achieved depends upon the extent to which the system can reduce the PSF, using either photo-switching or stimulated depletion. The increased resolution can be seen in images of microtubules (Fig 1D) and in the decreased FWHM in Table 1. However, assessing this can be difficult as the stimulated depletion can lead to a significant departure of the PSF from an Airy disk, particularly in systems with a pulsed excitation beam and continuous depletion beam (such as currently available commercial systems). These types of systems tend to have a temporal gate to prevent data collection for some period after the initial excitation, allowing the STED effect to mold the PSF. Unless extremely high depletion powers are used, there is some residual fluorescence in the periphery of the conventional PSF region during data collection. While the gate is open and data is actively collected, there is a large fluorescence signal from the central non-depleted region as well a smaller signal from the periphery. This leads to a PSF that is far from ideal, effectively with a bright STED spot superimposed on top of a weaker but much larger conventional PSF. The highly non-Gaussian nature of the resulting peak means that attempting to extract any meaningful measure from a simple Gaussian fit is unproductive. Adding more components does not help much since you run into significant signal to noise issues.

The resolution achieved in STED is often significantly better than that seen in SIM (see Table 1), but the very limited dynamic range and low S:N ratio mean that this is not easily visualized by Fourier Spectrum Analysis, where it is extremely difficult to see any signal beyond 0.2 um in the FFT image (Fig. 2D). In this case the radial integral clearly shows there is still real data out to at least 0.08 um (Fig. 3) but it is at an extremely low S:N level. Additionally, the gate length and depletion laser power are often tuned to enable collection of data in real samples where photo-bleaching is usually the major limiting factor. In this case users often reduce the depletion laser power, and then tweak the gate length to regain some of the lost resolution. In these cases the PSF is likely to be very far from Gaussian, giving systematic errors. STED data often have low signal levels, and therefore relatively low S:N levels, meaning the systematic deviation from a Gaussian is hidden by the low S:N.

Until recently, the commercial STED systems have only been able to do XY resolution enhancement, so the Z resolution will then be the same as a confocal image. The recent release of a commercial 3D STED system has enabled significant improvement in Z resolution, but at the expense of XY enhancement. The best balance between XY and Z resolution is then dependent upon the exact experimental situation, but enhanced Z resolution will limit XY resolution in almost all cases as the imaging is photon damage limited.

3.4.1. Single Molecule Localization Microscopy (SMLM)

The general class of SMLM techniques depend upon suppressing almost all the fluorophores in a sample, and imaging a very small fraction of fluorophores at a time. If only one fluorophore is emitting in a region significantly larger than the PSF, then the position of this single molecule can be localized to a precision much higher than the resolution of the system. After a large number of repeats, 1,000-100,000 or more, a large number of individual fluorophore positions can be acquired and a super-resolution image produced. Initial efforts using this technique focused on using photo-switching mechanisms to turn on and off individual molecules, but the field has largely moved on to using high illumination intensities (10-50 kW/cm^2), sometimes in combination with specific buffers [26], and relying on transferring a large percentage of molecules into a long-lived dark state. As they spontaneously return to a fluorescent state they are imaged, and then bleached or returned to a dark state. Fundamentally, all the SMLM techniques rely upon having low enough densities of single fluorescent molecules to be able to image them as a simple sum of individual PSFs. Higher density regions are rejected by the analysis routines and so produce no localizations. For similar reasons, background is a significant issue and so SMLM measurement are easiest, and usually performed, in Total Internal Reflection Fluorescence (TIRF) to minimize background and maximize S:N. However, the assignment of individual fluorophore positions allows delineation of structures that are often finer than any other methodology (Fig. 1E and Table 1)

3.4.2. Resolution in SMLM

Resolution in single molecule imaging is especially challenging. Many of the resolution measuring techniques used above are not simply transferable to SMLM

imaging. For instance, it is not robustly possible to apply Fourier Spectrum Analysis to a SMLM image, because the images are reconstructions, typically generated by cumulative plotting of perfect Gaussian kernels [27]. Unlike traditional microscopy images, these lack a distinct cutoff when analysed in the spatial frequency domain, implying an "infinite" resolution. (Fig. 2E and Fig. 3). Furthermore, doing FWHM curves on biological structures is likely to produce a number suspiciously close to the localization precision of the data points sampled. This is not the image resolution, but how accurately the few points that were averaged have been localized. Essentially, the resolution is defined not only by the localization precision, but also by the localization density. A structure that is not sufficiently detected cannot be defined. Therefore, the combination of labeling density and detection efficiency becomes increasing significant as the resolution improves. Some SMLM algorithms, such as fastSPDM, attempt to take this into account, and the results in Table 1 reflect this approach.

SMLM is particularly susceptible to these issues as it never detects all fluorescent molecules, and possibly detects very few. Exactly what fractions are detected, or are multiply detected, is often not known. This depends on a large number of factors (photophysics, mounting media, labeling efficiency, camera parameters) and cannot be theoretically derived but must rather be empirically determined [28,29]. Further, for SMLM, and dSTORM specifically, here is an additional noise component, due to multiple localizations of the same molecule, that is spatially structured and dominates the spectral power at high frequencies (25). Another significant issue in SMLM is how the analysis algorithm deals with overlapping fluorophores. In the best-case scenario, the separate molecules are fitted properly, each with an associated error. However, two close events in the same image, with high noise or low signal, can be indistinguishable from a single event. The event will then be assigned a position somewhere between the two real molecules with the position determined by the relative intensities from the two molecules. This generates images with artifacts such as bright objects linked by lines between them, or crossing filaments producing a webbed effect where the crossover point is smeared by arcs between the two filaments. This is a significant obstacle for any resolution-measuring technique that relies upon how closely two objects can be separated. Two close particles will tend to have a hump between them, and any measure from samples with two crossed filaments, *e.g.* microtubules or actin filaments, will tend to have an arched web between them. Both of these effects will reduce the measured resolution of the image compared to that gained from other measures such as the FWHM of a small object. However, if the resolution is defined by the Rayleigh Criterion, then this reduction will be real, as it is defined by how closely one can distinguish adjacent objects. These artifacts fundamentally reduce the ability to distinguish closely spaced objects in the image.

Another interesting approach to resolution in SMLM microscopy is Fourier Ring Correlation (FRC), a technique used in electron microscopy, but easily applied to SMLM imaging [30,31]. This relies upon separating the raw data localization positions randomly into two sets. These are separately Fourier-transformed and the correlation between the two at different distances is measured. This correlation determines how similar the two data sets are at that resolution, and therefore how closely different objects can be separated. The distance at which the correlation drops below some set value is defined as the resolution. However, while separating

the localizations in an independent manner is easy, other issues are not. Accurately correcting for the effect of multiple localization per molecule is difficult, as although a correction can be applied using only *a prioi* knowledge, the occurrence of multiple localizations cannot be reliably measured.

4. Conclusion

Resolution is a difficult concept, and the super-resolution techniques increase this complexity. The general concept of resolution is usually defined from the theoretical approach of the Rayleigh Criterion, whereas the practical approach is almost always to measure of the FWHM of some sub-resolution feature within the image (Table 1). This is a robust technique but it does not capture the same information as the theoretical approach and in some cases can significantly diverge in value. As discussed in the preceding sections (3.1-3.4) it is not trivial to compare practical measures from different techniques. The situation is further complicated by the fact that the theoretical measure is simply an arbitrary rule of thumb, if simply trying to distinguish a single particle from two, at some arbitrary separation then only a single addition piece of information is required and a resolution is limited purely by Signal:Noise [32], extremely high resolution can be generated as shown by SMLM techniques which effectively utilize this approach.

To properly assess the relative resolution of images from a number of techniques it is necessary to be able to analyze them in the same manner, and this is simply not possible given the different techniques and processing steps by which super resolution images are acquired. That said, significant information about the relative power of different techniques may still be usefully obtained. It is relatively easy to compare widefield and SIM images as they have similar image types, and dynamic ranges. The effective resolution can be compared from FWHM as calculated from Gaussian fits to sub-resolution features, or from comparing Fourier Transforms (Table 1, Fig. 3). From these sources it is clear that SIM achieves the stated doubling in resolution compared to widefield. Comparing widefield or SIM images to STED images is not easy. Although STED has the advantage of being the only direct super-resolution technique, its images often have extremely low dynamic range, and in some cases the point spread functions can be far from Gaussian (see section 3.3.1). Using a fitted Gaussian to estimate the FWHM gives a clear measure, but may underestimate the true resolution due to deviation of the point spread function from a Gaussian. Using Fourier Spectrum Analysis to estimate resolution is problematic in STED as well, due to its limited dynamic range and low signal at high frequencies (Fig. 2D). This results in STED seeming to have a lower practical resolution than commonly assumed (Fig. 3), but does not take into account its ability to resolve highly-contrasted structures at very high resolutions.

Finally, SMLM is the most difficult technique in which to assess resolution. The extremely high resolutions and ability to localize individual fluorophores mean that label density becomes a limiting factor [33]. The often low, and unknown, detection efficiency exacerbates this issue. Additionally, how the analysis software used deals with background, overlapping detections, drift, and a multitude of other issues can significantly affect image quality. Using Fourier Spectrum Analysis on the produced image is not possible, as the image is a construct with infinite resolution, and shows very slow decrease as resolution increases (Fig. 3). The recently published Fourier

Ring Correlation technique relies on being able to split the image into two independent sets, which is easy in SMLM imaging but very difficult in other super-resolution imaging techniques. It is thus a very useful technique for comparing between SMLM images but currently has little utility for comparisons between techniques. Further work may enable direct comparisons between FRC in SMLM techniques and Fourier Spectrum Analysis in other techniques, which will make cross-platform resolution comparisons more relevant.

Given the above points, the best approach to compare between techniques is still to perform the simple and robust fitting of a Gaussian to a sub-resolution object and then to extract the FWHM. However, the results should be handled with care. Issues such as label density, deviation of the PSF from a Gaussian and dynamic range limitations could significantly bias results. In SMLM it is particularly important not to replace real structural resolution with simple localization precision. Additionally, due to labeled density, local background and other issues, resolution may vary significantly across the image. In these cases, Fourier Spectrum Analysis may be helpful. It should also be noted that FWHM results are not necessarily comparable with the theoretical construct of the classical Rayleigh Criterion. There are no easy answers, and future work in both the fundamental optics and applied biological imaging fields should see tools developed to help resolve this cross-disciplinary impasse. Perhaps most importantly, researchers should remember that a “resolution number” shouldn’t be the primary deciding factor in which technique to use, and that they must be careful to define exactly what they mean when they quantify and compare resolution in super-resolution microscopy.

Figure Legends

Figure 1. Comparison of traditional and super-resolution microscopy data of immunofluorescently labeled microtubules in *Drosophila* macrophages. (A) Widefield image. (B) Widefield image after deconvolution. (C) 3D-SIM image after reconstruction. (D) STED image. (E) SMLM image at 2x magnification. All images are single Z-planes, and have been brightness/contrast adjusted for display. A-C generated from the same raw data. Scale bars: 5 μm (insets: 0.5 um). Inset boxes are at 4x magnification. (F) Line scans of representative single microtubules, from the positions shown by the circular blowups and the dotted lines in the images, demonstrating the relative resolutions of SIM, STED and SMLM images. Data points shown with Gaussian fits as the solid lines. All line scans are integrate over a 165nm width.

Figure 2. Fourier Spectrum Analysis of conventional and super-resolution microscopy data. Images are the FFT of the corresponding datasets in Figure 1. (A) Widefield image. (B) Widefield image after deconvolution. (C) SIM image after reconstruction. (D) STED image. (E) SMLM image. Radial position corresponds to inverse distance. The solid line represents a resolution of 0.3 μm, the dashed line a resolution of 0.2 μm, and the dotted line a resolution of 0.1 μm. Images A and B do not have frequency support beyond 0.2 μm. Note panels A-D are at the same scale while panel E has been scaled down to adequately show features in all images.

Figure 3. Fourier Spectrum Analysis of resolution. Inset: Schematic representing analysis method by integration of intensity along concentric rings of the Fourier

spectrum. Each expanding ring equates to an increase in resolution, and the intensities along each ring are averaged. Main image: Relative spectral amplitude of each microscopy method as resolution increases. Data are generated from the Fourier spectra in Fig. 2. Intensities are scaled to 100% in arbitrary units. The SMLM data is not readily comparable as discussed in section 3.4.2. Resolution along the x-axis is non-linear, as position in the Fourier spectrum corresponds to inverse distance.

Tables

Table 1. FWHM of microtubules, generated from images in Figure 1 and other similar images to get representative averages. Reported as mean ± standard deviation. n = 11 for SIM; n = 33 for gSTED; n = 11 for dSTORM.

Technique	FWHM
SIM	108 ± 5 nm
gSTED	63 ± 20 nm
dSTORM	42 ± 4 nm

Acknowledgement

This work was supported by the Wellcome Trust Strategic Award 091911, funding advanced microscopy at Micron Oxford. We thank: Christoffer Lagerholm at the Wolfson Imaging Centre Oxford for assistance with gSTED acquisitions; Rainer Kaufmann at Micron and Oxford's STRUBI for assistance with dSTORM acquisitions; Richard Parton and Ilan Davis at Micron Oxford.

References

[1] R. Han, Z. Li, Y. Fan, Y. Jiang, Recent advances in super-resolution fluorescence imaging and its applications in biology, J Genet Genomics. 40 (2013) 583–595. doi:10.1016/j.jgg.2013.11.003.

[2] L. Schermelleh, R. Heintzmann, H. Leonhardt, A guide to super-resolution fluorescence microscopy, The Journal of Cell Biology. 190 (2010) 165–175. doi:10.1083/jcb.201002018.

[3] R.M. Parton, A.M. Vallés, I.M. Dobbie, I. Davis, Live cell imaging in Drosophila melanogaster, Cold Spring Harb Protoc. 2010 (2010) pdb.top75–pdb.top75. doi:10.1101/pdb.top75.

[4] F. Grull, M. Kirchgessner, R. Kaufmann, M. Hausmann, U. Kebschull, Accelerating image analysis for localization microscopy with FPGAs, in: St International Conference on Field Programmable Logic and Application, 2011. doi:10.1109/FPL.2011.11.

[5] R. Kaufmann, J. Piontek, F. Grüll, M. Kirchgessner, J. Rossa, H. Wolburg, et al., Visualization and Quantitative Analysis of Reconstituted Tight Junctions Using Localization Microscopy, PLoS ONE. 7 (2012) e31128. doi:10.1371/journal.pone.0031128.

[6] J. Schindelin, I. Arganda-Carreras, E. Frise, V. Kaynig, M. Longair, T. Pietzsch, et al., Fiji: an open-source platform for biological-image analysis, Nature Methods. 9 (2012) 676–682. doi:10.1038/nmeth.2019.

[7] C.A. Schneider, W.S. Rasband, K.W. Eliceiri, NIH Image to ImageJ: 25 years

of image analysis, Nature Methods. 9 (2012) 671–675. doi:10.1038/nmeth.2089.
[8] L. Rayleigh, On the theory of optical images, with special reference to the microscope, Philosophical Magazine. 42 (1896) 167–195.
[9] G.B. Airy, On the diffraction of an object-glass with circular aperture, Transactions of the Cambridge Philosophical Society, 1835.
[10] C.M. Sparrow, On Spectroscopic Resolving Power, The Astrophysical Journal. 44 (1916) 76–86.
[11] C. Cremer, B.R. Masters, Resolution enhancement techniques in microscopy, Epj H. 38 (2013) 281–344. doi:10.1140/epjh/e2012-20060-1.
[12] M.G.L. Gustafsson, L. Shao, P.M. Carlton, C.J.R. Wang, I.N. Golubovskaya, W.Z. Cande, et al., Three-dimensional resolution doubling in wide-field fluorescence microscopy by structured illumination, Biophysical Journal. 94 (2008) 4957–4970. doi:10.1529/biophysj.107.120345.
[13] R. Heintzmann, C.G. Cremer, Laterally modulated excitation microscopy: improvement of resolution by using a diffraction grating, in: I.J. Bigio, H. Schneckenburger, J. Slavik, K. Svanberg, P.M. Viallet (Eds.), BiOS Europe '98, SPIE, 1999: pp. 185–196. doi:10.1117/12.336833.
[14] M.G.L. Gustafsson, Surpassing the lateral resolution limit by a factor of two using structured illumination microscopy, J Microsc. 198 (2000) 82–87. doi:10.1046/j.1365-2818.2000.00710.x.
[15] S.W. Hell, J. Wichmann, Breaking the diffraction resolution limit by stimulated emission: stimulated-emission-depletion fluorescence microscopy, Opt. Lett., OL. 19 (1994) 780. doi:10.1364/OL.19.000780.
[16] S.W. Hell, Far-field optical nanoscopy, 316 (2007) 1153–1158. doi:10.1126/science.1137395.
[17] M.A. Schwentker, H. Bock, M. Hofmann, S. Jakobs, J. Bewersdorf, C. Eggeling, et al., Wide-field subdiffraction RESOLFT microscopy using fluorescent protein photoswitching, 70 (2007) 269–280. doi:10.1002/jemt.20443.
[18] E. Betzig, G.H. Patterson, R. Sougrat, O.W. Lindwasser, S. Olenych, J.S. Bonifacio, et al., Imaging Intracellular Fluorescent Proteins at Nanometer Resolution, 313 (2006) 1642–1645. doi:10.1126/science.1127344.
[19] S.T. Hess, T.P.K. Girirajan, Ultra-high resolution imaging by fluorescence photoactivation localization microscopy, 91 (2006) 4258–4272. doi:10.1529/biophysj.106.091116.
[20] M.J. Rust, M. Bates, X. Zhuang, Sub-diffraction-limit imaging by stochastic optical reconstruction microscopy (STORM), 3 (2006) 793–796. doi:10.1038/nmeth929.
[21] L. Schermelleh, P.M. Carlton, S. Haase, L. Shao, L. Winoto, P. Kner, et al., Subdiffraction multicolor imaging of the nuclear periphery with 3D structured illumination microscopy, 320 (2008) 1332–1336. doi:10.1126/science.1156947.
[22] Z.R. Hoffman, C.A. DiMazrio, Structured illumination microscopy using random intensity incoherent reflectance, J Biomed Opt. 18 (2013) 061216. doi:10.1117/1.JBO.18.6.061216.
[23] R. Ayuk, H. Giovannini, A. Jost, E. Mudry, J. Girard, T. Mangeat, et al., Structured illumination fluorescence microscopy with distorted excitations using a filtered blind-SIM algorithm, Opt. Lett., OL. 38 (2013) 4723–4726.
[24] A.G. York, S.H. Parekh, D.D. Nogare, R.S. Fischer, K. Temprine, M. Mione,

et al., Resolution doubling in live, multicellular organisms via multifocal structured illumination microscopy, Nature Methods. 9 (2012) 749–754. doi:10.1038/nmeth.2025.
[25] A.G. York, P. Chandris, D.D. Nogare, J. Head, P. Wawrzusin, R.S. Fischer, et al., Instant super-resolution imaging in live cells and embryos via analog image processing, Nature Methods. 10 (2013) 1122–1126. doi:10.1038/nmeth.2687.
[26] N. Olivier, D. Keller, V.S. Rajan, P. Gönczy, S. Manley, Simple buffers for 3D STORM microscopy, 4 (2013) 885–899. doi:10.1364/BOE.4.000885.
[27] D. Baddeley, M.B. Cannell, C. Soeller, Visualization of Localization Microscopy Data, Microscopy and Microanalysis. 16 (2010) 64–72. doi:10.1017/S143192760999122X.
[28] E.J. Rees, M. Erdelyi, D. Pinotsi, A. Knight, D. Metcalf, Blind assessment of localisation microscope image resolution, Optical Nanoscopy. 1 (2012) 12. doi:10.1186/2192-2853-1-12.
[29] A.V. Abraham, S. Ram, J. Chao, E.S. Ward, R.J. Ober, Quantitative study of single molecule location estimation techniques, Opt Express. 17 (2009) 23352–23373. doi:10.1364/OE.17.023352.
[30] N. Banterle, K.H. Bui, E.A. Lemke, M. Beck, Fourier ring correlation as a resolution criterion for super-resolution microscopy, 183 (2013) 363–367. doi:10.1016/j.jsb.2013.05.004.
[31] R.P.J. Nieuwenhuizen, K.A. Lidke, M. Bates, D.L. Puig, D. Grünwald, S. Stallinga, et al., Measuring image resolution in optical nanoscopy, Nature Methods. 10 (2013) 557–562. doi:10.1038/nmeth.2448.
[32] G.T.D. Francia, Resolving Power and Information, J. Opt. Soc. Am. 45 (1955) 497–501. doi:10.1364/JOSA.45.000497.
[33] H. Deschout, F.C. Zanacchi, M. Mlodzianoski, A. Diaspro, J. Bewersdorf, S.T. Hess, et al., Precisely and accurately localizing single emitters in fluorescence microscopy, Nature Methods. 11 (2014) 253–266. doi:10.1038/nmeth.2843.

Figure 1

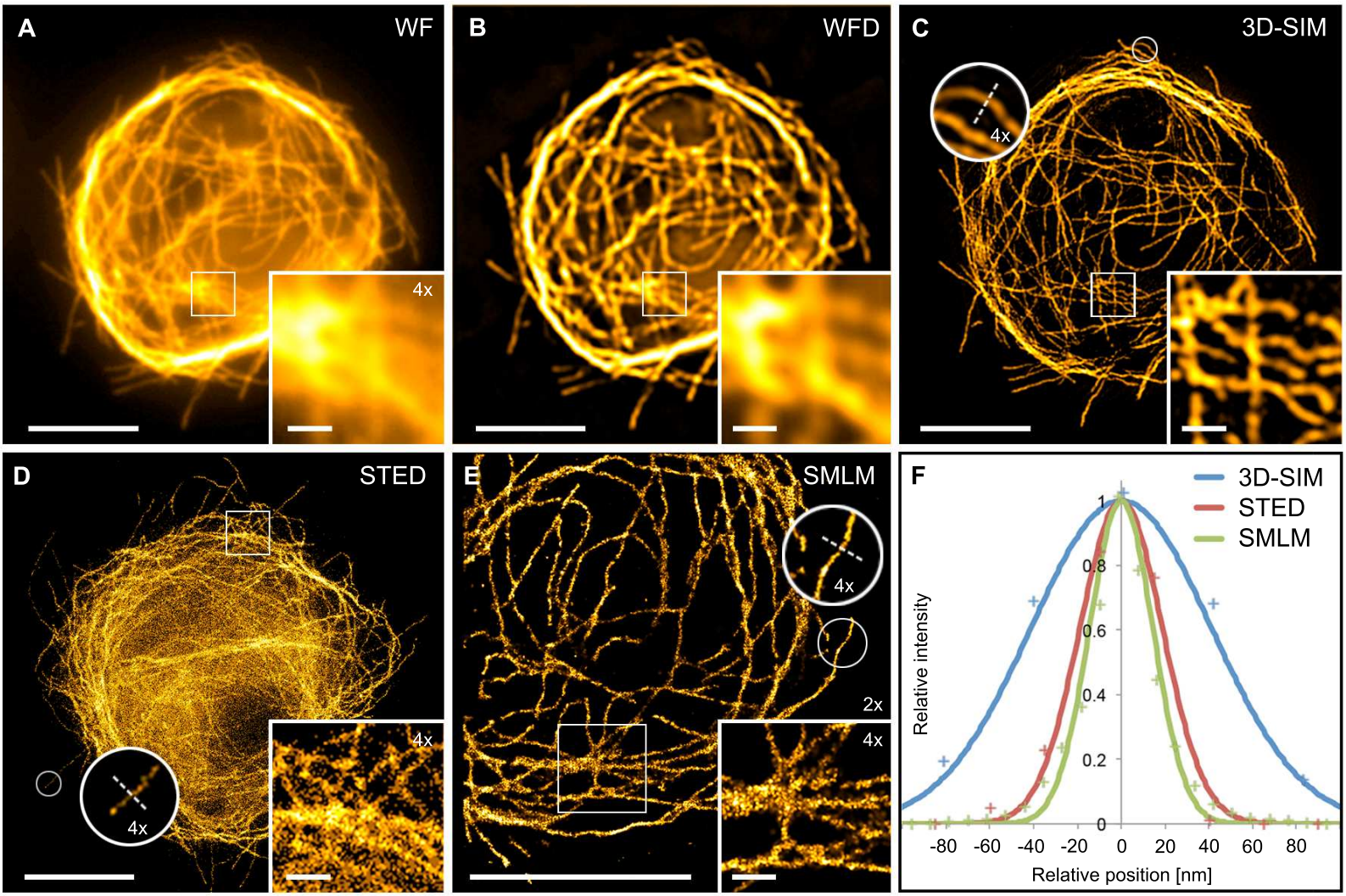
A
WF
4x
B
WFD
C
3D-SIM
4x
D
STED
4x
4x
E
SMLM
4x
2x
4x
F
3D-SIM
STED
SMLM
Relative intensity
1
0.8
0.6
0.4
0.2
0
-80
-60
-40
-20
0
20
40
60
80
Relative position [nm]

Figure 2

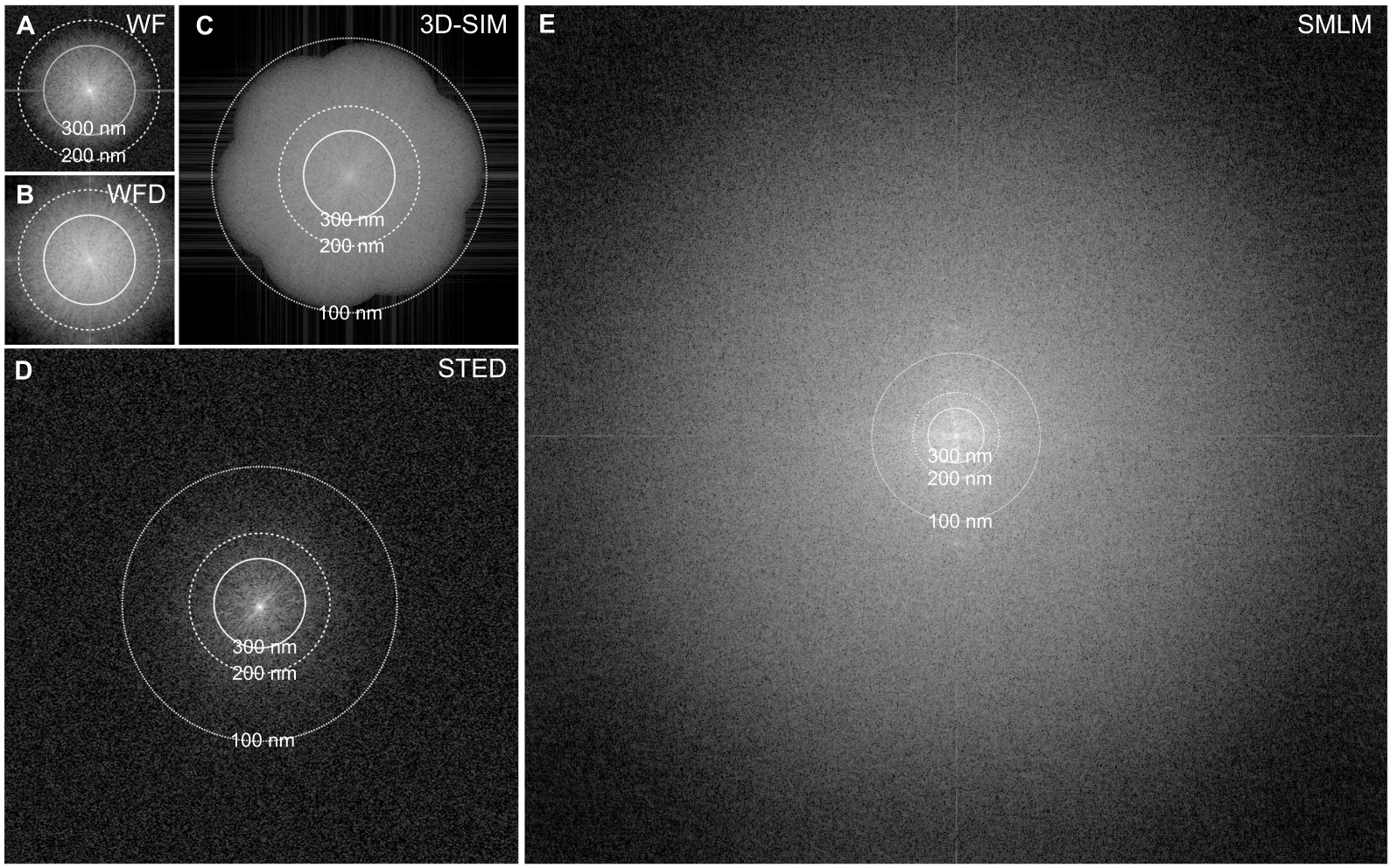
A
WF
300 nm
200 nm
B
WFD
C
3D-SIM
300 nm
200 nm
100 nm
D
STED
300 nm
200 nm
100 nm
E
SMLM
300 nm
200 nm
100 nm

Figure 3

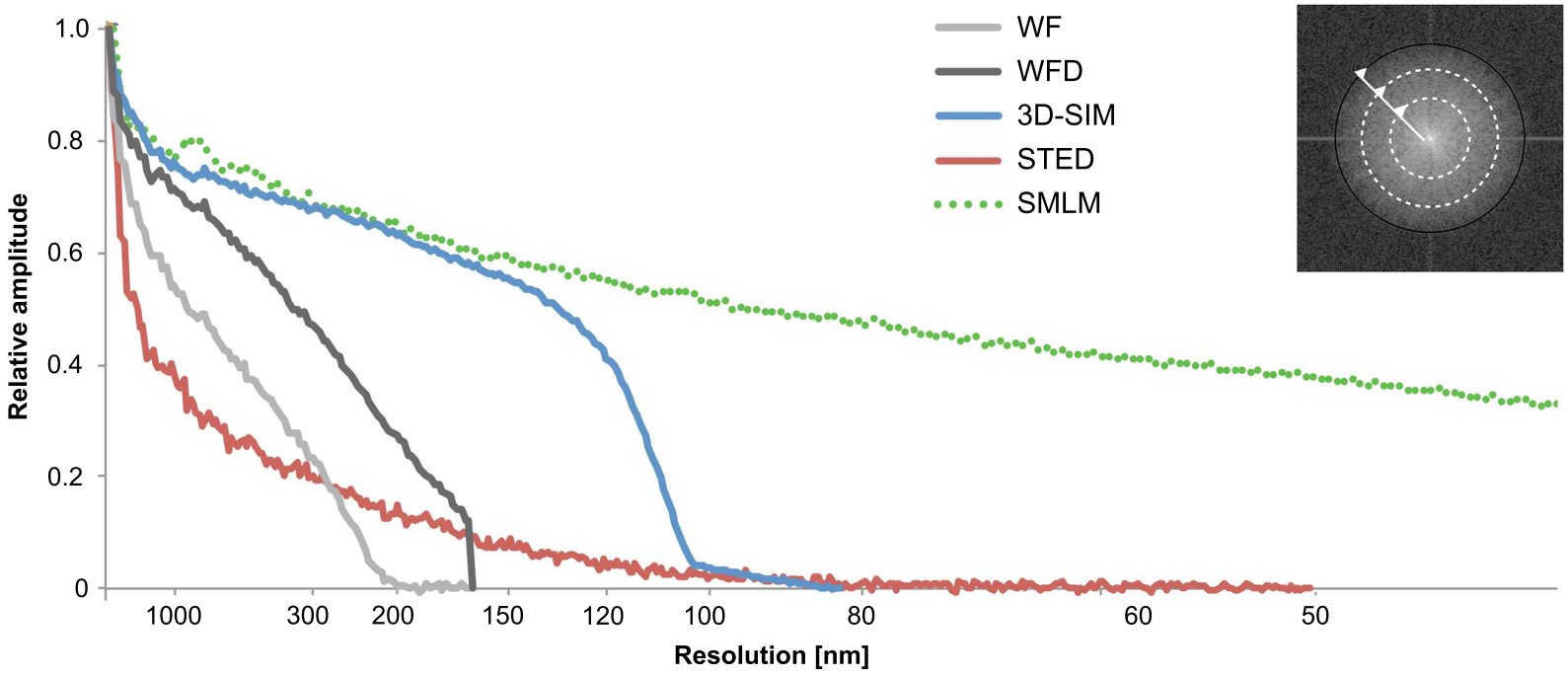
1.0
0.8
0.6
0.4
0.2
0
Relative amplitude
1000
300
200
150
120
100
80
60
50
Resolution [nm]
WF
WFD
3D-SIM
STED
SMLM